



Two-photon lasing by a superconducting qubit

P. Neilinger, M. Reháč, and M. Grajcar

*Department of Experimental Physics, Comenius University, SK-84248 Bratislava, Slovakia
and Institute of Physics, Slovak Academy of Sciences, 845 11 Bratislava, Slovakia*

G. Oelsner and U. Hübner

Leibniz Institute of Photonic Technology, P.O. Box 100239, D-07702 Jena, Germany

E. Il'ichev

Leibniz Institute of Photonic Technology, P.O. Box 100239, D-07702 Jena, Germany

and Novosibirsk State Technical University, 20 K. Marx Ave., 630092 Novosibirsk, Russia

(Received 8 January 2015; revised manuscript received 4 March 2015; published 19 March 2015)

We study the response of a magnetic-field-driven superconducting qubit strongly coupled to a superconducting coplanar waveguide resonator. We observed a strong amplification/damping of a probing signal at different resonance points corresponding to a one- and two-photon emission/absorption. The sign of the detuning between the qubit frequency and the probe determines whether amplification or damping is observed. The larger blue detuned driving leads to two-photon lasing, while the larger red detuning cools the resonator. Our experimental results are in good agreement with the theoretical model of qubit lasing and cooling at the Rabi frequency.

DOI: [10.1103/PhysRevB.91.104516](https://doi.org/10.1103/PhysRevB.91.104516)

PACS number(s): 42.50.Hz, 85.25.Am, 85.25.Cp, 85.25.Hv

Motivated by the first experiment demonstrating the energy exchange between a strongly driven superconducting qubit and a resonator at the Rabi frequency Ω_R [1], Hauss *et al.* [2] elaborated a theoretical model to quantify this phenomenon. Their model predicts large resonant effects for the one- and two-photon resonance conditions $\Omega_R = \omega_r - g_3 \bar{n}$ and $\Omega_R = 2\omega_r - g_3 \bar{n}$, where ω_r is the fundamental frequency of the resonator, g_3 is the effective coupling energy, and \bar{n} is the average number of photons in the resonator at frequency ω_r . Depending on the detuning between the driving frequency ω_d and the qubit eigenfrequency ω_q , either a lasing behavior (blue detuning $\omega_d - \omega_q > 0$) of the oscillator can be realized or the qubit can cool the oscillator (red detuning $\omega_d - \omega_q < 0$). According to the theory, one-photon lasing or cooling effects vanish at the symmetry (degeneracy) point of the qubit. However, the two-photon processes persist at the symmetry point where the qubit-oscillator coupling is quadratic and decoherence effects are minimized. There, the system realizes a “single-atom two-photon laser”. Note a similar two-photon lasing by a quantum dot in a microcavity, which was investigated theoretically in Ref. [3].

In optical many-atom systems, an amplification at the Rabi sidebands was already realized by Wu *et al.* [4] in the 1970s, and ten years later lasing was demonstrated by Khitrova *et al.* [5]. A single-atom laser has been demonstrated only recently by McKeever *et al.* [6]. In solid-state systems a single-qubit one-photon lasing was demonstrated by the NEC group [7]. Here, a single-charge qubit was used and a population inversion was provided by single-electron tunneling. Later on, the amplification/deamplification of a transmitted signal through a coplanar waveguide resonator was achieved by a strongly driven single-flux qubit [8]. However, two-photon lasing has not been experimentally demonstrated yet. In this paper, we report an experiment with strong indication for two-photon lasing, as well as a considerable enhancement of one-photon lasing of a superconducting qubit in comparison with Ref. [8]. The enhancement of 1 order of magnitude was

achieved by a much stronger coupling of the superconducting qubit to the resonator.

The lasing effect was investigated by making use of a standard arrangement: a superconducting qubit placed in the middle of a niobium $\lambda/2$ coplanar waveguide resonator. The latter was fabricated by conventional sputtering and dry etching of a 150-nm-thick niobium film. The patterning uses an electron-beam lithography and a CF_4 ion-etching process. The aluminum qubits were fabricated by the shadow evaporation technique. The coupling between the qubit and the resonator was implemented by a shared Josephson junction (Fig. 1). The dimensions of the qubit's Josephson junctions are $0.2 \times 0.3 \mu\text{m}^2$, $0.2 \times 0.2 \mu\text{m}^2$, and $0.2 \times 0.3 \mu\text{m}^2$, the critical current density is about $200 \text{A}/\text{cm}^2$, and the area of the qubit loop is $5 \times 4.5 \mu\text{m}^2$. The resonance frequency and the quality factor of the resonator's fundamental mode, taken for a weak probing ($p_p \approx -141 \text{ dBm}$), are $\omega_r = 2\pi \times 2.482 \text{ GHz}$, $Q_0 = 18000$. The same parameters of the third harmonics taken at the same power are $\omega_{r3} = 2\pi \times 7.446 \text{ GHz}$, $Q_3 = 3750$. These values were determined from the transmission spectra of the coplanar waveguide resonator.

In practice, we measured a two-qubit sample which represents a unit cell of a one-dimensional array of ferromagnetically coupled qubits exhibiting a large Kerr nonlinearity [9]. However, by applying a certain energy bias, one qubit can be set to a localized state, while the second is in the vicinity of its degeneracy point. This way, we can measure the qubits separately to reconstruct their parameters [10], and the dynamics of the system is defined by a single qubit only. Therefore, to describe our findings, we will use the one-qubit model elaborated in Ref. [2], in which the corresponding Hamiltonian reads as follows in the flux basis of the qubit:

$$H = -\frac{1}{2}\epsilon\sigma_z - \frac{1}{2}\Delta\sigma_x - \hbar\Omega_{R0}\cos(\omega_d t)\sigma_z + \hbar\omega_r a^\dagger a + g\sigma_z(a^\dagger + a), \quad (1)$$

where Δ is the energy-level separation of the two-level system at zero energy bias $\epsilon = 0$, Ω_{R0} is the driving amplitude of the

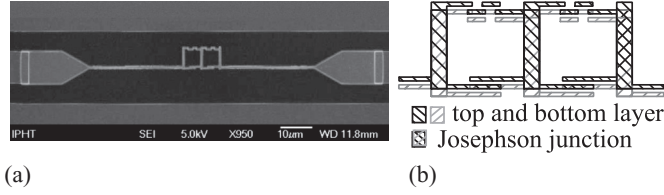


FIG. 1. (a) Scanning electron microscope image of the qubits incorporated into the coplanar waveguide resonator. (b) Detailed scheme of the qubits. The qubits share a Josephson junction with each other as well as with the resonator.

applied microwave magnetic flux with frequency ω_d , and g is the coupling energy between the qubit and the resonator. The coupling energy scales with the ratio of the magnitude of the persistent current in the qubit I_q and the critical current of the coupling Josephson junction I_{c0} as

$$g \equiv \hbar\omega_g = \frac{\hbar\omega_r}{2\pi} \frac{I_q}{I_{c0}} \sqrt{\frac{1}{G_0 Z_r}}, \quad (2)$$

where $Z_r = 50 \Omega$ is the wave impedance of the coplanar waveguide resonator and $G_0 \equiv 2e^2/h$ is the quantum conductance.

This Hamiltonian can be transformed by the Schrieffer-Wolff transformation $U = \exp(iS)$ with the generator $S = (g/\hbar\omega_q) \cos \eta (a + a^\dagger) \sigma_y$ and a rotating wave approximation $U_R = \exp(-i\omega_d \sigma_z t/2)$ to the following Hamiltonian [2]:

$$\begin{aligned} \tilde{H} = & \hbar\omega_r a^\dagger a + \frac{1}{2} \hbar\Omega_R \sigma_z \\ & + g \sin \eta [\sin \beta \sigma_z - \cos \beta \sigma_x] (a + a^\dagger) \\ & - \frac{g^2}{\hbar\omega_q} \cos^2 \eta [\sin \beta \sigma_z - \cos \beta \sigma_x] (a + a^\dagger)^2. \end{aligned}$$

Here, $\hbar\omega_q = \sqrt{\epsilon^2 + \Delta^2}$, $\Omega_R = \sqrt{\Omega_{R0}^2 \cos^2 \eta + \delta\omega^2}$, $\tan \eta = \epsilon/\Delta$, $\tan \beta = \delta\omega/(\Omega_{R0} \cos \eta)$, and $\delta\omega = \omega_d - \omega_q$. The transmission of the resonator

$$t \propto \langle a \rangle, \quad (3)$$

where

$$\langle a \rangle = \text{tr}(\tilde{\rho} a) \quad (4)$$

was calculated numerically by the quantum toolbox QUTIP [11], solving the Liouville equation for the density matrix of the system in the rotating frame,

$$\dot{\tilde{\rho}} = -\frac{i}{\hbar} [\tilde{H}, \tilde{\rho}] + \tilde{L}_q \tilde{\rho} + \tilde{L}_r \tilde{\rho}, \quad (5)$$

where \tilde{L}_q and \tilde{L}_r are Lindblad superoperators:

$$\begin{aligned} \tilde{L}_q \tilde{\rho} = & \frac{\tilde{\Gamma}_\downarrow}{2} (2\sigma_- \tilde{\rho} \sigma_+ - \tilde{\rho} \sigma_+ \sigma_- - \sigma_+ \sigma_- \tilde{\rho}) \\ & + \frac{\tilde{\Gamma}_\uparrow}{2} (2\sigma_+ \tilde{\rho} \sigma_- - \tilde{\rho} \sigma_- \sigma_+ - \sigma_- \sigma_+ \tilde{\rho}) \\ & + \frac{\tilde{\Gamma}_\varphi}{2} (\sigma_z \tilde{\rho} \sigma_z - \tilde{\rho}), \end{aligned} \quad (6)$$

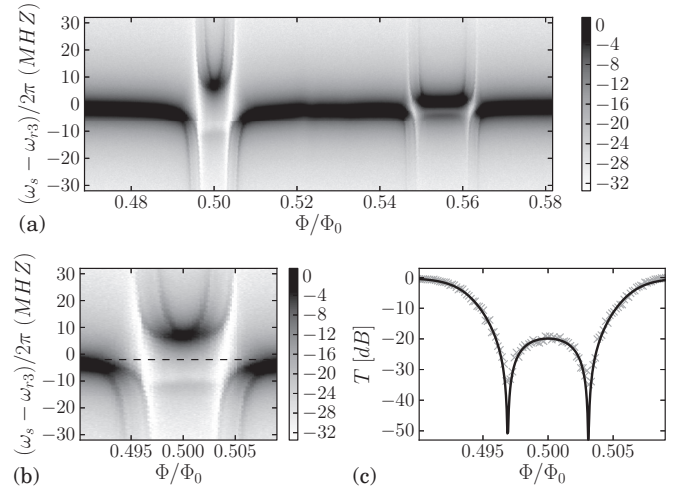


FIG. 2. (a) Resonator transmission as a function of the magnetic flux and the detuning of the resonator from the third harmonic resonance frequency $\omega_{r,3}/2\pi$. The anticrossings of qubits A and B are separated by a magnetic flux of about $55 \times 10^{-3} \Phi_0$. (b) Close view of the transmission in the vicinity of the left qubit's (A) degeneracy point and (c) the cut of the transmission map along the dashed line in (b). The crosses are experimental data and the solid line is a theoretical curve calculated from Eq. (9).

$$\begin{aligned} \tilde{L}_r \tilde{\rho} = & \frac{\kappa}{2} (N_{th} + 1) (2a \tilde{\rho} a^\dagger - \tilde{\rho} a^\dagger a - a^\dagger a \tilde{\rho}) \\ & + \frac{\kappa}{2} N_{th} (2a^\dagger \tilde{\rho} a - a a^\dagger \tilde{\rho} - \tilde{\rho} a a^\dagger). \end{aligned} \quad (7)$$

Here $N_{th} = 1/[\exp(\hbar\omega_T/k_B T) - 1]$ is the thermal distribution function of photons in the resonator, κ is resonator loss rate, and $\tilde{\Gamma}_{\downarrow, \uparrow}$ and $\tilde{\Gamma}_\varphi$ are the relaxation, excitation, and dephasing rates in the rotating frame derived in Ref. [2]:

$$\begin{aligned} \tilde{\Gamma}_{\uparrow, \downarrow} = & \frac{\Gamma_0}{4} \cos^2 \eta (1 \pm \sin \beta)^2 + \frac{\Gamma_\varphi}{2} \sin^2 \eta \cos^2 \beta, \\ \tilde{\Gamma}_\varphi = & \frac{\Gamma_0}{2} \cos^2 \eta \cos^2 \beta + \Gamma_\varphi \sin^2 \eta \sin^2 \beta. \end{aligned} \quad (8)$$

The qubit parameters used for the numerical calculations were determined independently from the transmission of the resonator t coupled to the undriven qubit. For a weak microwave signal with frequency ω_s , the transmission can be expressed in the simple form [12]

$$t = -i \frac{\kappa_{\text{ext}}}{2} \frac{\delta\omega_q + i\gamma}{\omega_g^2 \cos^2 \eta - (\delta\omega_r + i\kappa/2)(\delta\omega_q + i\gamma)}, \quad (9)$$

where $\delta\omega_q = \omega_q - \omega_s$, $\delta\omega_r = \omega_r - \omega_s$, κ_{ext} is the external loss rate of the resonator and γ is the QUBIT decoherence rate. The experimental data was fitted by Eq. (9) (see Fig. 2) and the QUBIT parameters obtained from the fitting procedure are given in Table I.

TABLE I. Qubit parameters determined from the fitting procedure.

Qubit	I_p (nA)	$\Delta/2\pi$ (GHz)	$g/2\pi$ (MHz)	$\gamma/2\pi$ (MHz)
A	208	6.39	109	15
B	138	5.28	77	20

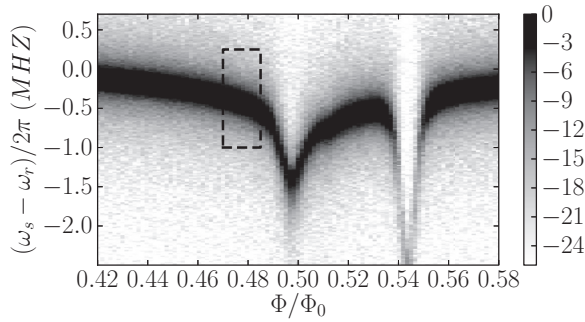


FIG. 3. (a) Resonator transmission in decibel units as a function of the magnetic flux and the detuning of the probe frequency from the resonance frequency 2.482 GHz.

We have investigated the stimulated emission effect observed when strongly driving the system at a frequency $\omega_d/2\pi = 9\omega_r/2\pi = 22.338$ GHz for qubit A. The resonator transmission was measured at weak probing signals p_p by a network analyzer at resonance ω_r for a magnetic flux in the area marked by the black rectangular area in Fig. 3. The corresponding normalized average photon number \bar{n}/\bar{n}_0 in the resonator is shown in Fig. 4(a). Here we follow the definition used in Ref. [2] where, for high photon numbers, $\bar{n} = \langle a \rangle \langle a^\dagger \rangle$

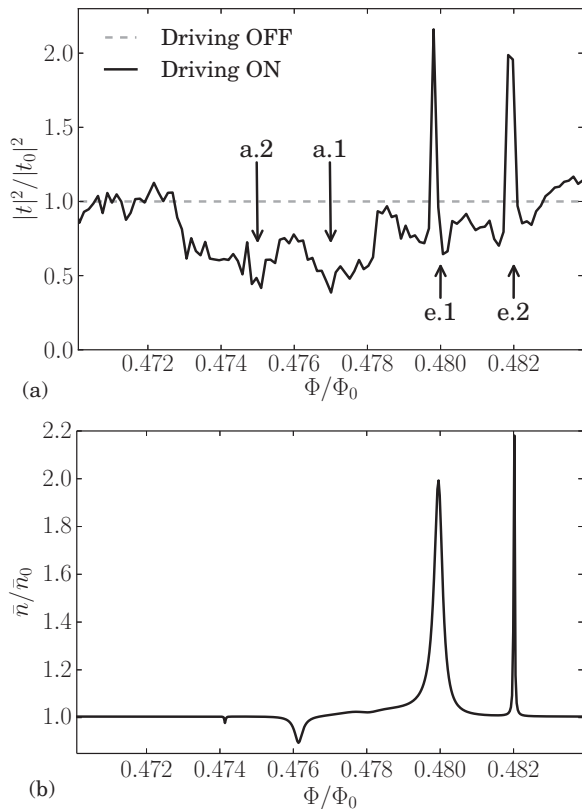


FIG. 4. Normalized transmission of the resonator $|t|^2/|t_0|^2$ at fixed frequency $\omega_s/2\pi$ for driving signal with frequency $\omega_d/2\pi = 9\omega_r/2\pi = 22.338$ GHz and power $p_d = -102$ dBm for the driving switched off and on (a). Regions $e.1$, $e.2$ and $a.1$, $a.2$ exhibit amplification and attenuation of the signal, respectively. Panel (b) shows the simulated average photon number in the resonator obtained for the qubit parameters.

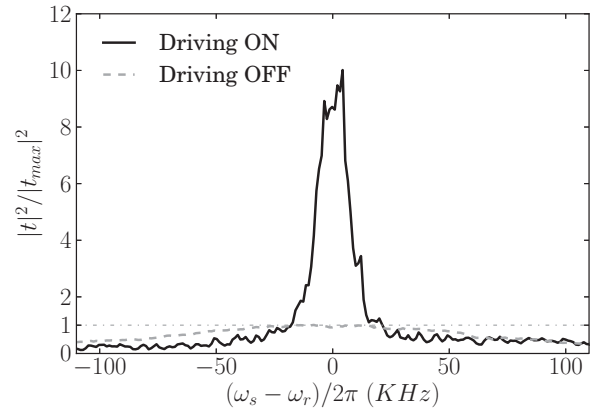


FIG. 5. Normalized resonance curve of the resonator at driving switched off (dashed line) and on (solid line) with frequency $\omega_d/2\pi = 9\omega_r/2\pi = 22.338$ GHz and power $p_d = -101$ dBm in region $e.1$. The amplitude increases by a factor of ~ 9 and bandwidth is reduced by a factor of 10.

and \bar{n}_0 are the average photon number in the resonator with and without driving, respectively. Note that the normalized photon number \bar{n}/\bar{n}_0 and the normalized transmission $|t|^2/|t_0|^2$, where t_0 is the resonator transmission without driving, provide the same quantity.

At a driving power $P_d = -103$ dBm, two emission peaks ($e.1$, $e.2$) accompanied by two attenuation dips ($a.1$, $a.2$) appear in the transmission spectra. The increase of the transmission is accompanied by a narrowing of the resonance curve. The one-photon ($a.1$, $e.1$) and two-photon ($a.2$, $e.2$) processes are enhanced at resonance with the Rabi frequency of the qubit $\Omega_R = \omega_r - g_3\bar{n}$ and $\Omega_R = 2\omega_r - g_3\bar{n}$, respectively. As Fig. 4(b) shows, these results are in good agreement with the theoretical model [2] described above for parameters given in Table I. By a strong coupling of the qubit to the resonator, we have achieved a considerable enhancement of the lasing, nearly 1 order of magnitude (see Fig. 5), in comparison with the results presented in Ref. [8]. Further improvement is possible by increasing the relaxation rate of the qubit, for instance, by placing a gold resistor close to the qubit loop.

To conclude, we have demonstrated an experiment with strong indication for single-qubit one-photon and two-photon lasing. The experimental results are in good agreement with the theoretical model developed by Hauss *et al.* [2]. The considerable enhancement of the lasing effect was achieved by stronger coupling of the superconducting qubit to the resonator, and theoretical calculations show that it can be enhanced further by increasing the relaxation rate of the qubit. Such improvement could enable one to observe even the higher-order processes analyzed in Ref. [13].

The research leading to these results was supported by funding from the European Community's Seventh Framework Program (FP7/2007-2013) under Grant No. 270843 (iQIT). This work was also supported by the Slovak Research and Development Agency under Contracts No. APVV-DO7RP003211, No. APVV-0515-10, No. APVV-0808-12 (former Projects No. VVCE-0058-07 and No. APVV-0432-07), and No. LPP-0159-

09. The authors gratefully acknowledge the financial support of the EU through the European Commission's ERDF OP R&D, Projects CE QUTE ITMS: 26240120009 and CE METAQUTE

ITMS: 26240120022. E.I. acknowledges partial support from the Russian Ministry of Education and Science, within the framework of State Assignment 8.337.2014/K.

-
- [1] E. Il'ichev, N. Oukhanski, A. Izmalkov, T. Wagner, M. Grajcar, H.-G. Meyer, A. Y. Smirnov, A. Maassen van den Brink, M. H. S. Amin, and A. M. Zagoskin, *Phys. Rev. Lett.* **91**, 097906 (2003).
- [2] J. Hauss, A. Fedorov, C. Hutter, A. Shnirman, and G. Schön, *Phys. Rev. Lett.* **100**, 037003 (2008).
- [3] E. del Valle, S. Zippilli, F. P. Laussy, A. Gonzalez-Tudela, G. Morigi, and C. Tejedor, *Phys. Rev. B* **81**, 035302 (2010).
- [4] F. Y. Wu, S. Ezekiel, M. Ducloy, and B. R. Mollow, *Phys. Rev. Lett.* **38**, 1077 (1977).
- [5] G. Khitrova, J. F. Valley, and H. M. Gibbs, *Phys. Rev. Lett.* **60**, 1126 (1988).
- [6] J. McKeever, A. Boca, A. D. Boozer, J. R. Buck, and H. J. Kimble, *Nature (London)* **425**, 268 (2003).
- [7] O. Astafiev, K. Inomata, A. O. Niskanen, T. Yamamoto, Y. A. Pashkin, Y. Nakamura, and J. S. Tsai, *Nature (London)* **449**, 588 (2007).
- [8] G. Oelsner, P. Macha, O. V. Astafiev, E. Il'ichev, M. Grajcar, U. Hübner, B. I. Ivanov, P. Neilinger, and H.-G. Meyer, *Phys. Rev. Lett.* **110**, 053602 (2013).
- [9] M. Reháč, P. Neilinger, M. Grajcar, G. Oelsner, U. Hübner, E. Il'ichev, and H.-G. Meyer, *Appl. Phys. Lett.* **104**, 162604 (2014).
- [10] E. Il'ichev, N. Oukhanski, T. Wagner, H.-G. Meyer, A. Smirnov, M. Grajcar, A. Izmalkov, D. Born, W. Krech, and A. Zagoskin, *Low Temp. Phys.* **30**, 620 (2004).
- [11] J. Johansson, P. Nation, and F. Nori, *Comput. Phys. Commun.* **184**, 1234 (2013).
- [12] A. N. Omelyanchouk, S. N. Shevchenko, Y. S. Greenberg, O. Astafiev, and E. Il'ichev, *Low Temp. Phys.* **36**, 893 (2010).
- [13] S. N. Shevchenko, G. Oelsner, Y. S. Greenberg, P. Macha, D. S. Karpov, M. Grajcar, U. Hübner, A. N. Omelyanchouk, and E. Il'ichev, *Phys. Rev. B* **89**, 184504 (2014).